Bioorganic Chemistry 87 (2019) 560–571

Contents lists available at ScienceDirect

Bioorganic Chemistry

journal homepage: www.elsevier.com/locate/bioorg

Antiproliferative effect, cell cycle arrest and apoptosis generation of novel synthesized anticancer heterocyclic derivatives based 4*H*-benzo[*h*] chromene

Fawzia F. Alblewi[a,*], Rawda M. Okasha[a], Zainab M. Hritani[a], Hany M. Mohamed[b,c], Mohammed A.A. El-Nassag[b,c], Ahmed H. Halawa[c], Ahmed Mora[c], Ahmed M. Fouda[d], Mohammed A. Assiri[d], Al-Anood M. Al-Dies[d], Tarek H. Afifi[a], Ahmed M. El-Agrody[c]

[a] Chemistry Department, Faculty of Science, Taibah University, 30002 Al-Madinah Al-Munawarah, Saudi Arabia
[b] Chemistry Department, Faculty of Science, Jazan University, Jazan 45142, Saudi Arabia
[c] Chemistry Department, Faculty of Science, Al-Azhar University, Nasr City 11884, Cairo, Egypt
[d] Chemistry Department, Faculty of Science, King Khalid University, Abha, 61413, P.O. Box 9004, Saudi Arabia

ARTICLE INFO

Keywords:
Antiproliferative
Cell cycle analysis
Cell apoptosis
SAR study
Chromene derivatives

ABSTRACT

Novel *β*-enaminonitrile/ester compounds (**4**, **6**) and an imidate of **4** (**9**) were utilized as key scaffolds for the synthesis of newly 2-substituted 4*H*-benzo[*h*]chromene (**7**, **8, 10, 11, 13, 14**) and 7*H*-benzo[*h*]chromeno[2,3–*d*] pyrimidine derivatives (**15–19**). The spectral data confirmed the successful isolation of the desired compounds. The targeted compounds were assessed for their *in vitro* anticancer activity against mammary gland breast cancer cell line (MCF-7), human colon cancer (HCT-116), and liver cancer (HepG-2), while doxorubicin, vinblastine, and colchicine were utilized as standard references drugs. Some of the examined compounds displayed high growth inhibitory activity against the three different cell lines. For example, the aminoimino derivative (**18**) exhibited excellent antitumor activity versus all cancer cell lines with IC_{50} values = 0.45 μg/mL, 0.7 μg/mL, and 1.7 μg/mL. Among the tested molecules, compounds **9**, **15**, and **18** were selected for further study regarding their effects on cell cycle analysis, apoptosis assay, caspase 3/7 activity, and DNA fragmentation. We found that these three potent cytotoxic compounds induce cell cycle arrest at the S and G2/M phases, which causes apoptosis. Furthermore, these compounds significantly inhibit the invasion and migration of the different tested cancer cells. Finally, the SAR survey highlighted the antitumor activity of the new molecules that was remarkably influenced by the hydrophilicity of substituent as well the fused rings at certain positions.

1. Introduction

Chromene molecules have been recognized as one of the most focal drug candidates that are largely presented in natural products or obtained via synthetic origin. This class of molecules exhibits a wide assortment of remarkable biological activities. Their low toxicity in association with their broad pharmacological properties has enthused chemists to search for new medicinal agents. A large number of chromene and benzochromene derivatives have been designed with attractive biological properties, such as antimicrobial activities [1–4], anti-influenza drug discovery programmes [5], anti-inflammatory effects [6,7], antioxidant properties [8], Alzheimer's disease treatments [9,10], and the prevention of sugar cataracts that can instigate human blindness [11]. The variety and significance of the properties of the chromene and fused chromene derivatives have been emphasized in several reviews and articles for the manufacturing of potent antitumor agents [12–14].

In general, all of the biological properties of the chromene compounds have been developed through the modification of the pyran olefin in order to enhance the properties of a particular lead structure or to increase the library diversity. For instance, several modifications including epoxidation, hydrogenation, dihydroxylation, and amino hydroxylation have been employed to produce a massive number of biologically active chromene derivatives.

(Fig. 1) is a representative example of different chromene systems as promising candidates that can be utilized as drug targets for cancer treatment [15–23]. For example, Compound (**A**) exhibited an antagonistic behaviour against cancer cells, establishing selective

* Corresponding author.
E-mail address: fbalawi@taibahu.edu.sa (F.F. Alblewi).

https://doi.org/10.1016/j.bioorg.2019.03.059
Received 17 December 2018; Received in revised form 14 February 2019; Accepted 19 March 2019
Available online 22 March 2019
0045-2068/

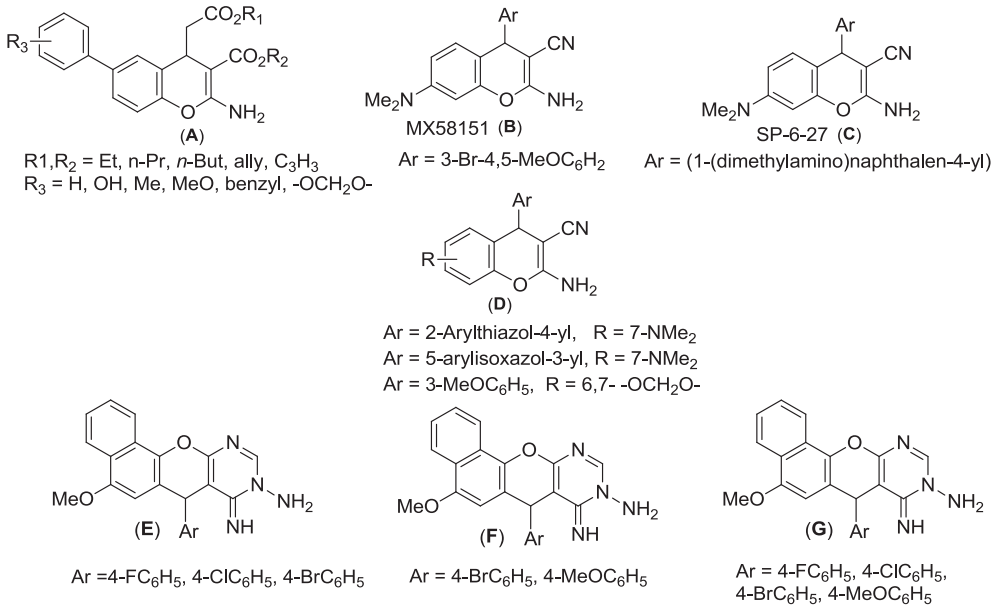

Fig. 1. Biological activities of lead chromene analogues.

cytotoxicity towards malignant cells [15,16], low cytotoxicity against a wide range of hematologic solid tumour cells [17,18], and enhanced the activity of the human promyelocytic leukemia and multidrug-resistant variant (HL60/MX2) cell line. Meanwhile, the 2-amino-7-dimethylamino-4-aryl-4*H*-chromene-3-carbonitrile (**B**) displayed growth inhibition of the multidrug-resistant human uterine sarcoma (MES-SA/DX-5) [19]. Compound (**C**) was active against melanoma, and prostate cancer cell lines [20] while compound (**D**) showed the highest strength towards the nasopharyngeal epidermoid carcinoma cell line (KB), which is a rare type of head and neck cancer, human primary medulloblastoma (DAOY) cell line, human brain astrocytoma (1321N1) cell line and acts as potent antimitotic agents [21–23]. On the other hand, the 7*H*-benzo[*h*]chromeno[2,3-*d*]pyrimidine moiety exhibited anticancer activities. For example, the compounds (**E, F** & **G**) have significantly more potent antitumor activity against different human cancer cell lines, as presented in (Fig. 1), [24–27].

Furthermore, 1*H*-benzo[*f*]chromene moieties have emerged as one of the most auspicious and desirable scaffolds for the development of potent antitumor agents. For instance, several derivatives of 1*H*-benzo[*f*]chromene, compounds (**H, I, J** & **K**), exhibited promising cytotoxic and apoptotic effects on various cancer cell lines, as shown in (Fig. 2), [2,28–31].

The previous findings have served as motivation for the design and synthesis of a novel *β*-enaminonitrile/ester and chromenopyrimidine derivatives with the primary aim of developing agents with potential antiproliferative activity towards various human cancer cell lines. The DNA damage checkpoint operates as a monitor that detects potentially harmful DNA-damaged cells, then triggers the activation of apoptosis induction to block carcinogenesis [32]. The present study also examines the mechanisms underlying the cytotoxicity of the most potent compounds, utilizing cell cycle analyses, annexin V assay, caspase 3/7 activity, and DNA fragmentation while taking into consideration the cancer cell invasion and migration. The SAR of the novel compounds accentuated the influence of the substituents at different positions on the antitumor activity.

2. Results and discussion

2.1. Chemistry

The route adopted for the preparation of compounds **4**, **6–11**, and **13–19** is described in Scheme 1–5. The synthesis was prompted by microwave irradiation of 4-methoxy-1-naphthol (**1**) with 3,4-dimethoxybenzaldehyde (**2**), $CH_2(CN)_2$ (**3**), and/or $CNCH_2CO_2Et$ (**5**) in EtOH/piperidine solution. The reactions proceeded at 140 °C for 2 min. to furnish the *β*-enaminonitrile (**4**) and *β*-enaminoester (**6**), respectively. The optical activity of *β*-enaminonitrile/ester was determined using a Carl Zeiss polarimeter, which revealed zero rotation (i.e., optical inactivity) and, therefore, the formation of a racemic (±) mixture, as shown in Scheme 1, [27,33].

The structure and purity of compounds **4** and **6** were confirmed by the spectral data. The IR spectra of the target compounds **4** and **6** confirmed the presence of the characteristic NH_2 absorption bands at υ 3386, 3331, 3215 and υ 3412, 3310 cm^{-1} while the CN and CO absorption bands appeared at υ 2193 and 1676 cm^{-1}, respectively. On the other hand, the ^1H NMR spectra of **4** and **6** showed the singlet signals of the amino, methine, and methoxy protons at δ 7.05, δ 4.79, δ 3.72, δ 3.71 and δ 7.72, δ 4.99, δ 3.73, δ 3.66 ppm, respectively. In addition, the methylene, the methyl protons resonated at δ 4.02 and δ 1.16 ppm for compound **6** while the ^{13}C NMR spectra of **4** and **6** showed signals

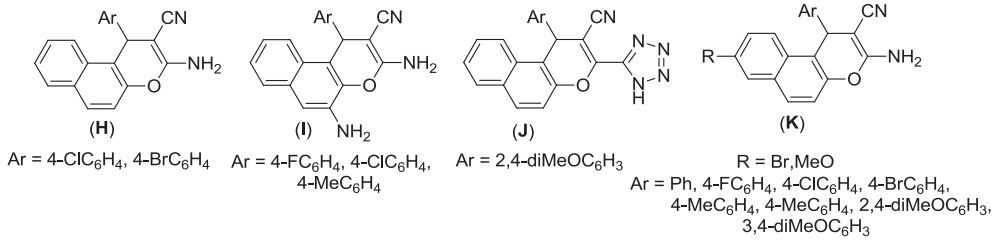

Fig. 2. Structure of selected 1*H*-benzo[*f*]chromene derivatives.

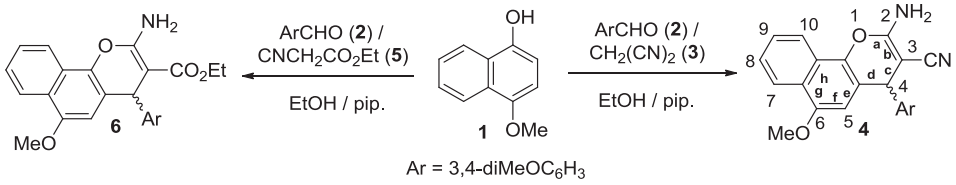

Scheme 1. Synthesis of *β*-enaminonitrile/ester (4, 6).

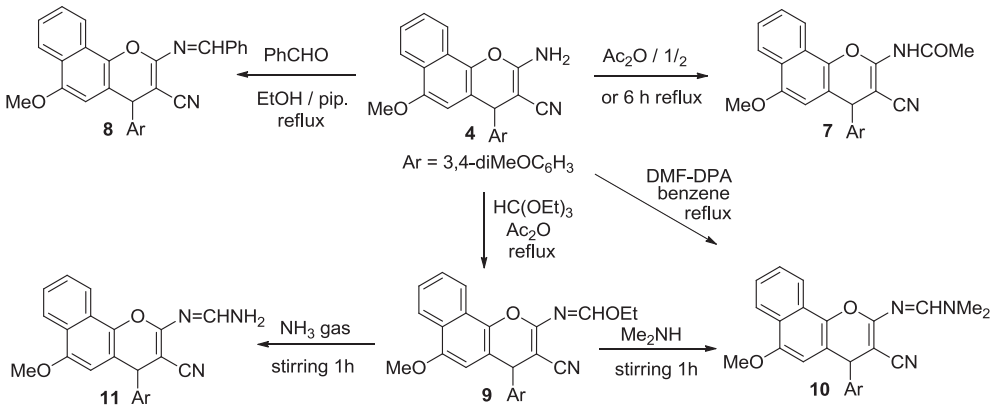

Scheme 2. Synthetic protocol of 2-substituted *β*-enaminonitrile (7–11).

resonating at *δ* 41.72, *δ* 56.23, *δ* 56.15 and *δ* 39.93, *δ* 55.46, *δ* 55.37 ppm, which is attributed to the methine and methoxy carbons, respectively. Furthermore, the two peaks at *δ* 58.55 and *δ* 14.36 ppm are corresponding to the methylene and methyl carbons, compound **6**.

The synthesis of the 2-substituted 4*H*-benzo[*h*]chromene derivatives (**7–10**) was achieved via the reaction of *β*-enaminonitrile (**4**) with different nucleophilic reagents, namely, acetic anhydride, benzaldehyde, triethyl orthoformate, and *N,N*-dimethylformamide dineopentyl acetal (DMF-DPA), while the ammonolysis of compound **9**, via the stirring of bubbling ammonia gas in MeOH at ambient temperature for 1 h, resulted in the production of an open chain 2-aminomethyleneamino-4-(3,4-dimethoxyphenyl)-6-methoxy-4*H*-benzo[*h*]chromene-3-carbonitrile (**11**) as shown in Scheme 2.

The spectroscopic data (IR, ^{1}H NMR, ^{13}C NMR) and the elemental analyses were consistent with either structure. The IR spectra of **7–11** exhibited the disappearance of the NH_2 group of *β*-enaminonitrile and the appearance of the NH and CO absorption bands at *υ* 3250 and *υ* 1700 cm^{-1} for compound **7**. The ^{1}H NMR spectra of compounds **7–11** displayed singlet signals, resonating at *δ* 2.15 ppm for the acetyl protons of compound **7** and the olefinic protons around *δ* 9.40–8.10 ppm for compounds **8–11**. Moreover, the ^{13}C NMR spectra of **7–11** exhibited the acetyl carbon at *δ* 25.10 ppm for compound **7** and the olefinic carbons around *δ* 160.97–157.60 ppm for compounds **8–11.**

Similarly, the reaction of *β*-enaminoester (**6**) with triethyl orthoformate or DMF-DPA afforded the desired product, 2-formamido derivative (**13**) instead of imidate (**12**) and/or the amidine (**14**), respectively Scheme 3.

Compound **13** was formed via the addition of H_2O to the imidate of **12**, which eliminates an EtOH molecule and forms the 2-formamido derivative **13**, Scheme 3, [24].

The IR spectra of compounds **13** and **14** revealed the disappearance of the NH_2 group of *β*-enaminoester and the appearance of NH and CO

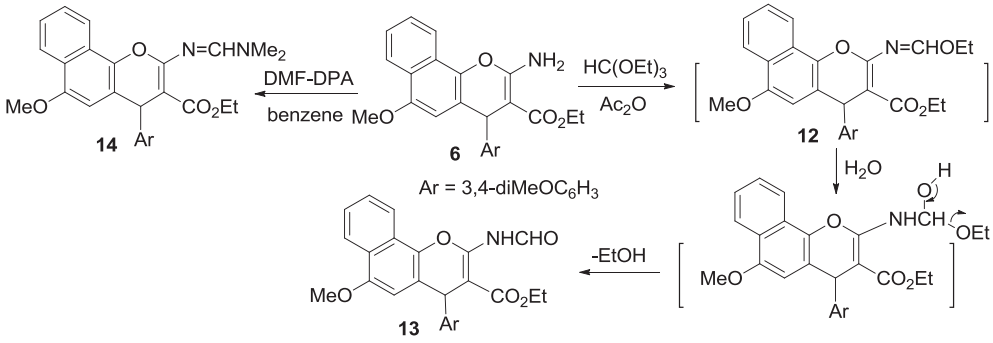

Scheme 3. Synthetic protocol of ethyl 2-formamido and amidine compounds (13, 14).

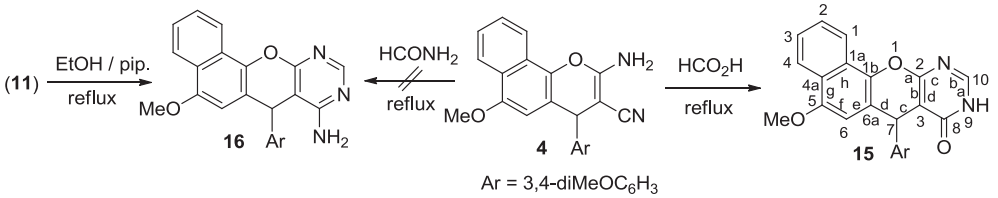

Scheme 4. Synthesis protocol of the chromenopyrimidine derivatives (15, 16).

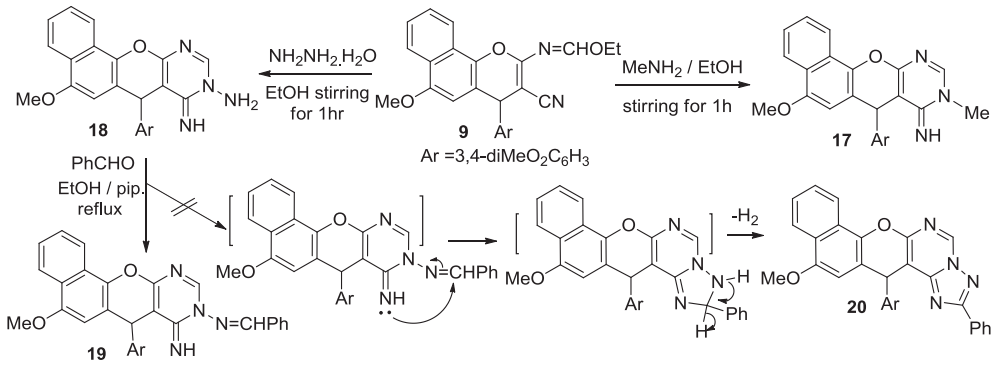

Scheme 5. Synthesis protocol of compounds 17–19.

of the formyl absorption bands at υ 3400 and υ 1676 cm^{-1}, compound **13**. On the other hand, the ^{1}H NMR spectra of compounds **13** and **14** showed singlet signals as a result of the existence of the formyl, imino protons for compound **13** and the olefinic proton for compound **14** at δ 10.58, δ 10.75 ppm and δ 8.21 ppm, respectively. The methylene and methyl protons showed signals at δ 4.08, δ 4.00 and δ 1.18, δ 1.17 ppm for compound **13** and **14**. The ^{13}C NMR spectra of **13** and **14** exhibited signals of the formyl and olefinic carbonyl carbons at δ 166.46 and δ 155.85 ppm, respectively, while the methylene and methyl carbons resonated at δ 60.00, δ 58.82 and δ 13.96, δ 14.17 ppm, respectively.

Compounds **4** and **9** are successful precursors for the synthesis of an assortment of novel heterocyclic derivatives based on 4*H*-benzo[*h*] chromene. Therefore, the condensation of molecule **4** with formic acid afforded pyrimidine derivative (**15**), while the reaction of **4** with formamide, following the same methodology, was unsuccessful in forming 8-aminopyrimidine derivative (**16**). However, the cyclization of **11** in a refluxed ethanolic piperidine solution successfully synthesized compound **16,** as shown in Scheme 4, [34]. The IR spectra of compounds **15** and **16** revealed the disappearance of the NH_2 and CN groups of β-enaminonitrile and the appearance of NH and CO absorption bands at υ 3500 and υ 1766 cm^{-1} for compound **15** and the NH_2 group at υ 3475, 3414, 3309 cm^{-1} for compound **16**. The ^{1}H NMR spectra of compounds **15** and **16** showed singlet signals, resulting from the pyrimidine proton at δ 8.21, δ 8.21 ppm and the NH and NH_2 protons at δ 7.90 and 6.75 ppm, respectively. The ^{13}C NMR spectrum of **15** exhibited the signal of the carbonyl carbon at δ 164.00 ppm.

The interaction of the imidate **9** with the methylamine or hydrazine hydrate was done at room temperature in methanolic solution for 1 h and afforded the cycloaddition product of iminopyrimidine (**17**) and aminoiminopyrimidine derivatives (**18**), respectively, while the condensation of the amino group in **18** with the benzaldehyde in piperidine/EtOH solution produced the Schiff base open product 9-benzylideneaminopyrimidine derivative (**19**) instead of the cycloaddition compound (**20**), as shown in Scheme 5. The IR spectra of compounds **17–19** revealed three imino absorption bands around υ 3340–3210 cm^{-1} as well as the NH_2 absorption bands at υ 3315, 3168 cm^{-1}, compound **18**. The ^{1}H NMR spectra showed the NH and pyrimidine protons, ranging from δ 9.70–6.80 ppm and δ 8.20–7.69 ppm, respectively. Furthermore, the NH_2 protons of compound **18** and the olefinic proton of compound **19** revealed singlet signals at δ 5.70 and δ 8.42 ppm, respectively. The ^{13}C NMR spectrum of **19** exhibited the signal of the olefinic carbon at δ 151.49 ppm. Moreover, the ^{13}C NMR-DEPT spectra at 45°, 90°, 135° and the ^{13}C NMR-APT of compound **17** gave an absolute confirmation for the structure of **17**.

It is also vital to mention that the 4-position of compounds **4**, **6–11**, **13**, **14**, and the 7-position of compounds **15–19** are chiral centres. The target compounds were characterized using IR, NMR and Mass spectra and were included in Tables 1 & 2 in the Supplementary materials as well the elemental analysis.

2.2. Biological evaluation

2.2.1. In vitro cytotoxic activity

The target compounds **4**, **6–11**, **13**, **14**, and **15–19** were assessed for their cytotoxic effects towards MCF-7, HCT-116, and HepG-2 cell lines. The selection of these particular cell lines and standard drugs was stimulated by the affirmed antitumor effects of reported chromene, benzochromene and benzochromenopyrimidine derivatives [12–31,33,35–38]. The cytotoxic activity was appraised using the 3-(4,5-dimethylthiazol-2-yl)-2,5-diphenyl tetrazolium bromide (MTT) colorimetric assay [39,40]. The *in vitro* cytotoxicity evaluation was achieved under different concentrations (50, 25, 12.5, 6.25, 3.125, 1.56 and 0 μg/mL), doxorubicin, vinblastine, and colchicine were used as reference cytotoxic drugs. The outcomes were conveyed as growth inhibitory concentration (IC_{50}) values, as shown in (Fig. 3) and Table 1.

From Table 1, it was noticeable that some of the synthesised compounds exhibited superior to modest antiproliferative activity against the various human cell lines. In particular, compounds **18** and **11** (IC_{50} = 0.45 μg/mL and 3.8 μg/mL, respectively) were displayed the most potent counterparts, as they were 13.6 and 1.6 times more active than vinblastine (IC_{50} = 6.1 μg/mL) and 39.3 and 4.7 times more active than colchicine (IC_{50} = 17.7 μg/mL), respectively, while compound **18** was equipotent to doxorubicin (IC_{50} = 0.4 μg/mL) against MCF-7. Furthermore, compounds **8**, **7**, **15**, and **16** displayed good activities against the MCF-7 cell line, with IC_{50} values of 8.1, 8.4, 9.7 and 11.5 μg/mL, respectively, in comparison to colchicine (IC_{50} = 17.7 μg/mL). On the other hand, compounds **18** and **9**, with IC_{50} values of 0.7 μg/mL and 2.2 μg/mL, respectively, were more active against HCT-116 than vinblastine and colchicine (IC_{50} = 2.6 μg/mL and 42.8 μg/mL), and compounds **15**, **11**, **6**, **7**, **16**, **8**, **17**, and **4,** with IC_{50} values ranging from 4.2 to 37 μg/mL, exhibited a higher cytotoxic effect compared to colchicine while compound **18** (IC_{50} = 0.7 μg/mL) was almost equipotent to doxorubicin (IC_{50} = 0.5 μg/mL) against HCT-116. Additionally, compound **9** (IC_{50} = 0.7 μg/mL) exhibited superior activity against the HepG-2 cancer cell line in comparison to the reference drugs (IC_{50} = 0.9 μg/mL, 4.6 μg/mL, and 10.6 μg/mL), while compounds **18** and **15**, with IC_{50} = 1.7 μg/mL and 4.4 μg/mL, respectively, possessed excellent antiproliferative activities against HepG-2 cells compared to vinblastine and colchicine (IC_{50} = 4.6 μg/mL and 10.6 μg/mL); furthermore, compounds **7** and **17** (IC_{50} = 4.8 μg/mL and 5.9 μg/mL) had better activity than colchicine against the same cell line. Overall, the other compounds were moderately active or had weak activity in comparison to the reference drugs.

2.2.2. Cell cycle analysis

The impact of the synthesized compounds on the regulation of the cell cycle progression was explored using the Propidium Iodide Flow Cytometry Kit assay. Changes in the cell cycle were detected after the incubation of the MCF-7, HCT-116, and HepG-2 cells with compounds **9**, **15**, and **18**, selected for their potent cytotoxic activities in 24 h. The

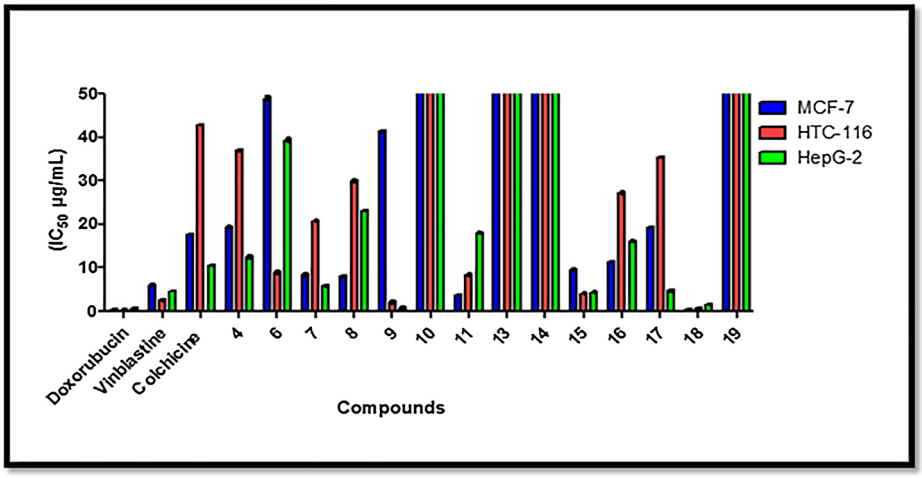

Fig. 3. IC_{50} values (µg/mL) of benzo[*h*]chromenes and chromeno[2,3–*d*]pyrimidines derivatives against three cancer cells.

representative cell cycle distribution histogram of the stained DNA of the cancer cells treated with different compounds is shown in (Fig. 4a). These results demonstrated that compounds **9** and **15** produced a significant increase in the capture of cancer cells in the cell population at the S and G2/M phases for the MCF-7, HCT-116, and HepG-2 treated cells in comparison to the untreated cells. Compound **18** displayed the highest accumulation of cells at the G2/M phase when compared to compounds **9** and **15**; however, it did not affect the cell population in the S phase, as shown in (Fig. 4b). The distribution of cells in the G1 phase notably decreased in comparison to the control cells. The cell cycle evaluation revealed that the tested compounds significantly halted the progression of cells by restricting both the S and G2/M phases. This action can correlate with the fact that the drug-stabilized topoisomerase-DNA non-cleaved complexes efficiently inhibit DNA synthesis or repair [41,42].

2.2.3. Cell apoptosis

The phosphatidylserine (PS) translocation from the inside to the surface of the cell membrane is widely accepted as a marker for apoptosis [43]. Therefore, the Annexin V/PI double staining flow cytometric assay was utilized for the further evaluation of the cell death pathway induced with the assessed compounds. The dot plot flow cytometry data of the stained cells with the Annexin V-FITC and PI is displayed in Fig. 5a.

Table 1
Outcome of cytotoxic activity.

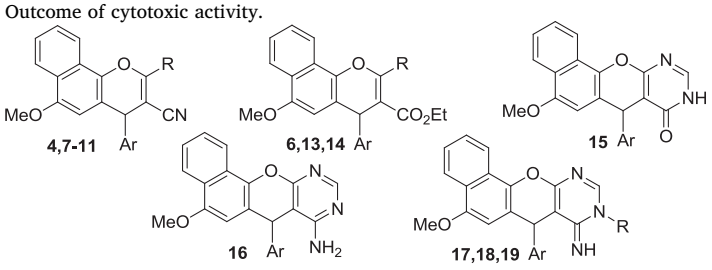

Compound	R	IC_{50} (µg/mL)[a]		
		MCF-7	HCT-116	HepG-2
4	NH_2	19.4 ± 0.15	37.0 ± 0.25	12.5 ± 0.3
6	NH_2	49.0 ± 0. 5	9.0 ± 0.25	39.4 ± 0.4
7	NHAc	8.4 ± 0.23	20.9 ± 0.23	5.9 ± 0.11
8	N=CHPh	8.1 ± 0.2	30.0 ± 0.3	23.2 ± 0.1
9	N=CHOEt	41.5 ± 0.14	2.2 ± 0.3	0.7 ± 0.4
10	$N{=}CHNMe_2$	w	w	w
11	$N{=}CHNH_2$	3.8 ± 0.11	8.4 ± 0.31	18.1 ± 0.07
13	NHCHO	w	w	w
14	$N{=}CHNMe_2$	w	w	w
15	–	9.7 ± 0.2	4.2 ± 0.1	4.4 ± 0.12
16	–	11.5 ± 0.01	27.3 ± 0.16	16.2 ± 0.16
17	Me	19.5 ± 0.02	35.6 ± 0.05	4.8 ± 0.06
18	NH_2	0.45 ± 0.03	0.7 ± 0.08	1.7 ± 0.01
19	N=CHPh	w	w	w
Vinblastine	–	6.1 ± 0.03	2.6 ± 0.08	4.6 ± 0.01
Colchicine	–	17.7 ± 0.01	42.8 ± 0.02	10.6 ± 0.04
Doxorubicin	–	0.4 ± 0.01	0.5 ± 0.02	0.9 ± 0.04

[a] IC_{50} values (µg/mL) as the mean values of triplicate wells from at least three experiments, reported as the mean ± standard error. w = weak activity ($IC_{50} \geq 50$ µg/mL).

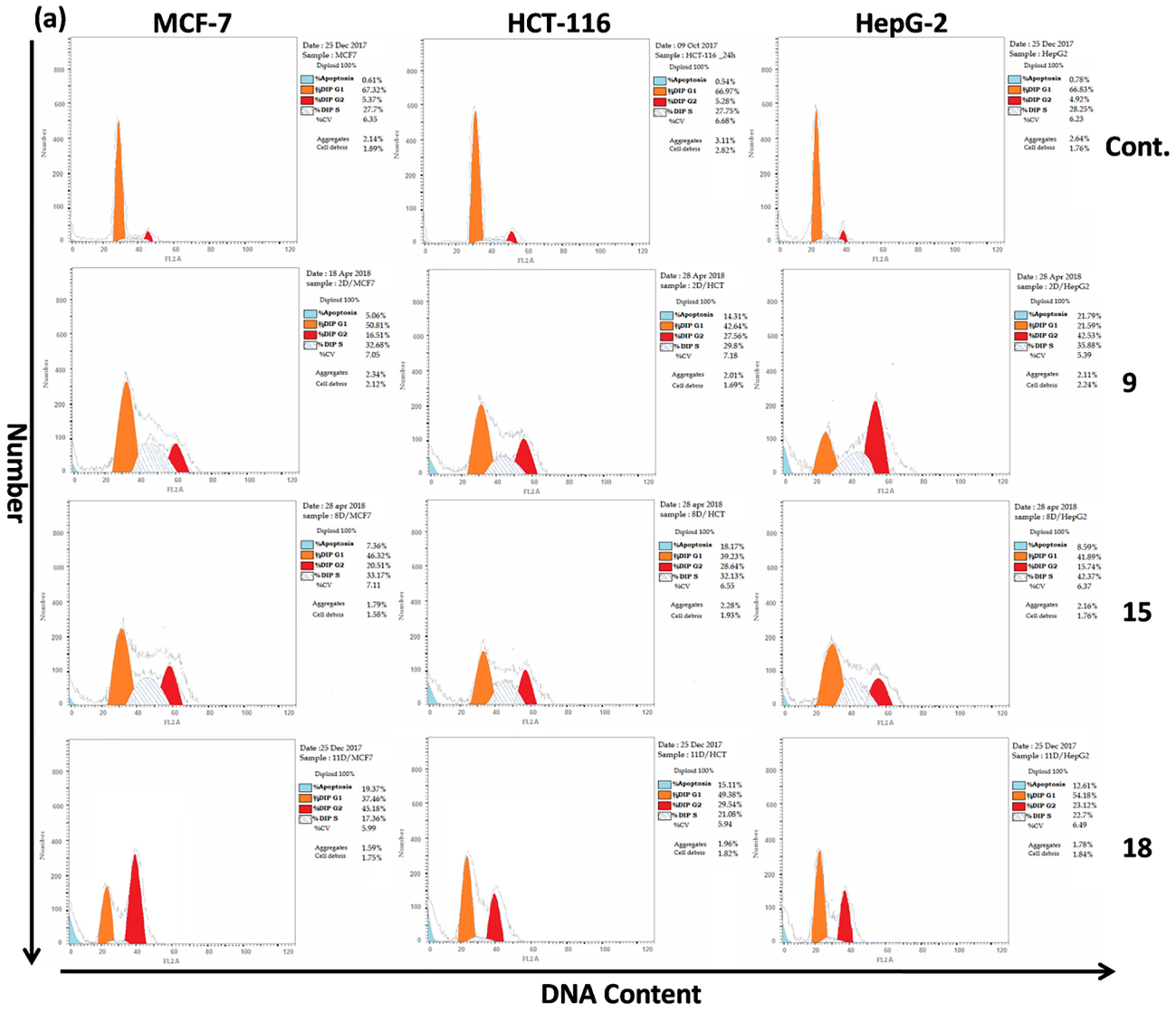

Fig. 4a. Representative histograms of DNA content distribution of cell cycle phases of three cell lines treated with compounds 9, 15 and 18 (4 μg/mL) for 24 h. DNA content was stained with (PI).

The Annexin V/PI double staining disclosed that after 24 h of exposure, MCF-7, HCT-116, and HepG-2 cells had undergone early and late apoptosis when treated with compounds **9**, **15**, or **18** compared to untreated control cells. The proportion of total apoptosis in the case of MCF-7 treated with compound **18** was highly efficient compared to the other two compounds, as shown in (Fig. 5b). Necrosis was not observed in any of the treated conditions, indicating that cell death occurred primarily through apoptosis. Unlike necrosis, apoptotic cells do not release their cellular content into the interstitial tissue, which triggers an inflammatory response that causes the collateral destruction of normal cells in the surrounding microenvironment [44].

2.2.4. Caspase 3/7 activity

The major apoptotic pathways include the extrinsic (death receptor), the intrinsic (mitochondrial), and the perforin/granzyme pathways [45]. For the further investigation of the apoptotic

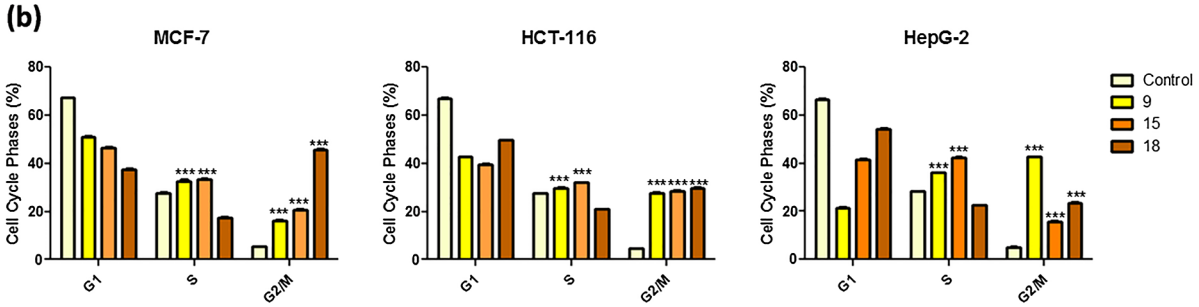

Fig. 4b. Percentage of three cell lines in the G1, S, and G2/M phases after incubation with compounds 9, 15, and 18 (4 μg/mL) for 24 h. The results are expressed as the mean ± SD of three independent experiments in triplicate. Significances are shown in comparison to control cells ($^{*}p < 0.05$; $^{**}p < 0.01$; $^{***}p < 0.001$).

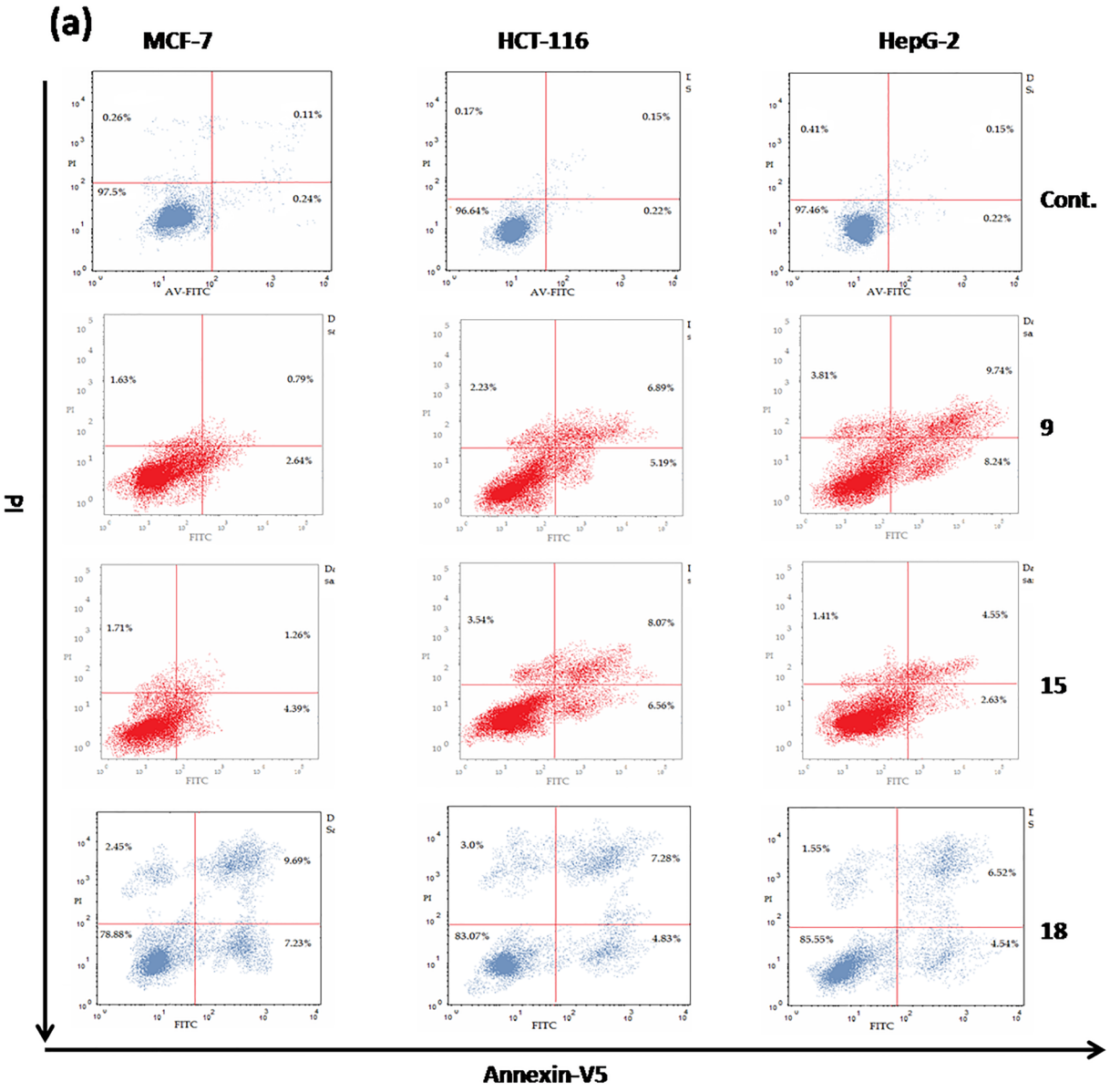

Fig. 5a. Dot plot of Annexin V/PI stained cells treated with the indicated drugs for 24 h.

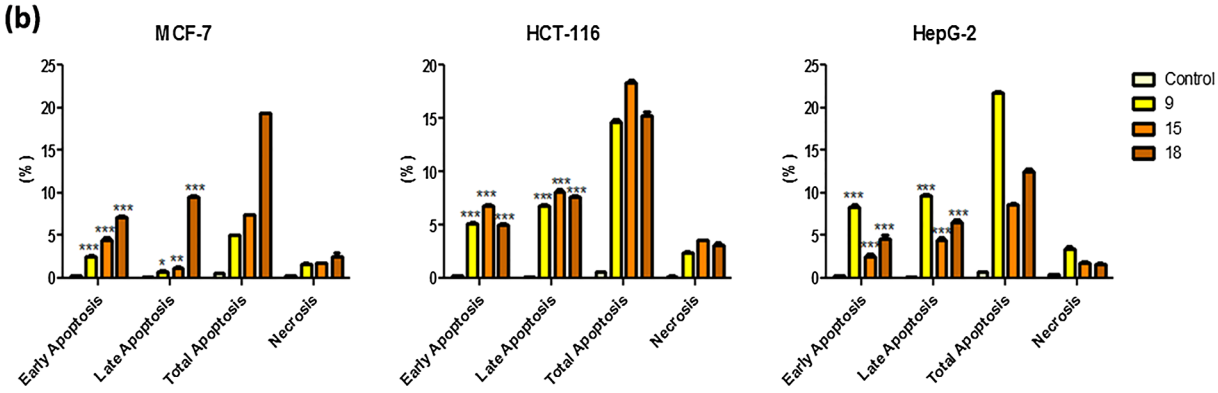

Fig. 5b. Apoptosis percentage of three cell lines after incubation with compounds 9, 15 and 18 (4 μg/mL) for 24 h. The data are expressed as the mean ± SD of three independent experiments in triplicate. Significance is shown in comparison to control cells ($^{*}p < 0.05$; $^{**}p < 0.01$; $^{***}p < 0.001$).

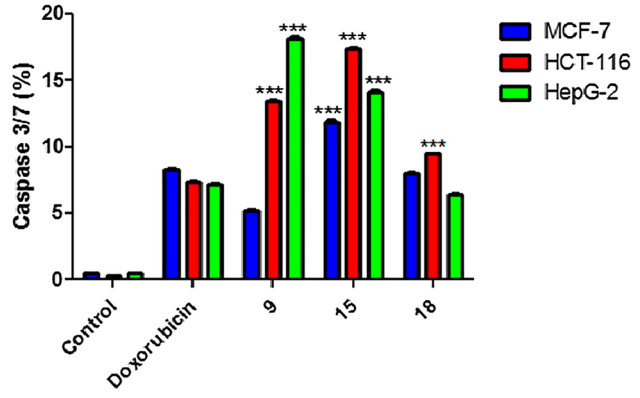

Fig. 6. Caspase 3/7 activity percentage of three cell lines after incubation with compounds 9, 15 and 18 (4 μg/mL) for 24 h. The data are expressed as the mean ± SD of three independent experiments in triplicate. Significance is shown in comparison to doxorubicin treated cells ($^{*}p < 0.05$; $^{**}p < 0.01$; $^{***}p < 0.001$).

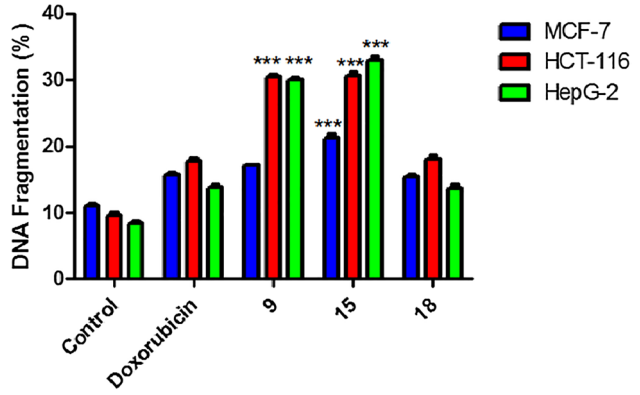

Fig. 7. DNA fragmentation percentage of three cell lines after incubation with compounds 9, 15, and 18 (4 μg/mL) for 24 h. The data are expressed as the mean ± SD of three independent experiments in triplicate. Significance is shown in comparison to doxorubicin treated cells ($^{*}p < 0.05$; $^{**}p < 0.01$; $^{***}p < 0.001$).

mechanism induced by the tested compounds, the caspase 3/7 activity was evaluated using the Cell Event™ Caspase 3/7 Green Detection kit. The levels of caspase 3/7 in the MCF-7 cells treated with compounds **9** (5.15%), **15** (11.83%), and **18** (8.02%) were generally equivalent to doxorubicin (8.28%). Compounds **9** and **15** significantly increased the level of caspase 3/7 in the case of HCT-116 cells (13.46% and 17.36%, respectively) and HepG-2 cells (18.16% and 14.13%, respectively), which doubled the levels obtained by doxorubicin for both cell lines. Compound **18** exhibited equipotent caspase 3/7 activity levels to doxorubicin against HCT-116 and HepG-2 (Fig. 6). These results confirm the induction of the caspase-dependent apoptotic pathway by the examined compounds.

2.2.5. DNA fragmentation

The degradation of the nuclear DNA into nucleosomal units is the earliest and most characterized biochemical event that is common to all processes of apoptosis in a caspase-dependent manner [46,47]. The relative quantity of the DNA fragments in the cells treated with compounds **9**, **15**, **18**, and doxorubicin is displayed in (Fig. 7). The degree of the DNA fragmentation increased considerably in all cells that were treated with compounds **9** and **15** compared to doxorubicin. No difference in the DNA fragmentation was witnessed between the cells treated with compound **18** or doxorubicin. These results integrate with the outcomes of the caspase activity which were previously presented in Table 1.

2.2.6. Cell invasion and migration

Metastasis is responsible for the greatest number of cancer deaths. The cell cycle results have improved the possibility that the tested compounds might influence cell invasion and migration. Compounds **9**, **15**, and **18** showed significantly reduced cell invasion (Fig. 8a) and migration (Fig. 8b) in all experimented cells compared to untreated cells. The interphase microtubule-dependent activities perform a focal role in cell invasion/migration through numerous pathways [48,49]. The possible effect of the tested compounds on the microtubule polymerization or depolymerization might be the reason for the demonstrated data.

2.2.7. Structure activity relationship (SAR) studies

Examining all previous results, we can deduce valuable data regarding the SAR of the new chromene systems. The effect of the substitution at different positions on the antitumor activities of the target compounds has been explored. The activity against the MCF-7 cell line, with the merging of a pyrimidine ring at the 2, 3-positions that contains hydrophobic group (=NH group at position 8, $-NH_2$ group at position 9) in compound **18** displayed a decreased IC_{50} value. The same trend has been shown for the 4*H*-benzo[*h*]chromene compounds **7** and **11** with the hydrophobic substituents, −NHCOMe, and N=$CHNH_2$, at the 2-position with the −CN-3.

We then extend our investigation towards the impact of the substitution of the 2-position with $-CN/CO_2Et$-3 or the pyrimidine ring at the 2, 3-positions of the synthesized 4*H*-benzo[*h*]chromene on the activity against the HCT-116 cell line. Among all the prepared derivatives, compounds **4**, **6–11**, **13**, and **14**, with a hydrophobic group such as −N=CHOEt at the 2-position, exhibited high inhibitory action against the HCT-116 cells. Meanwhile, compounds **15** and **18** with the pyrimidine ring at the 2, 3-positions and a hydrophobic group, such as = NH-8 or $-NH_2$-9, exhibited a strong activity against the HCT-116 cell

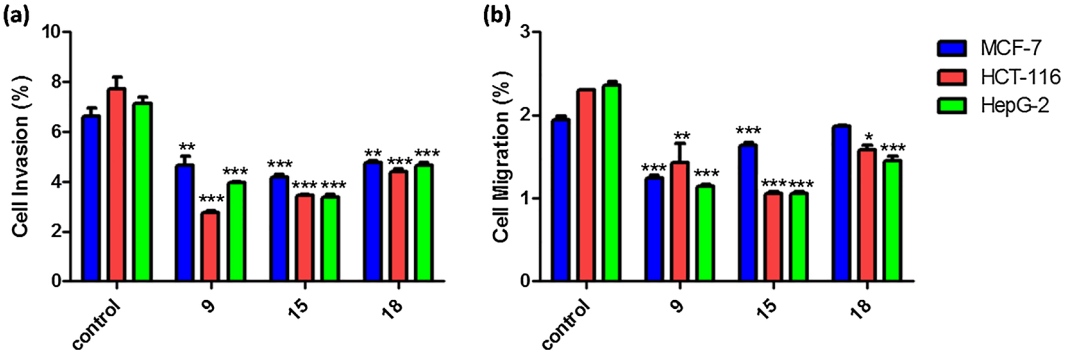

Fig. 8. Cell (a) invasion and (b) migration percentage of three cell lines after incubation with compounds 9, 15, and 18 (4 μg/mL) for 24 h. The data are expressed as the mean ± SD of three independent experiments in triplicate. Significance is shown in comparison to control cells ($^{*}p < 0.05$; $^{**}p < 0.01$; $^{***}p < 0.001$).

line relative to the other substituted analogues. Regarding the effect of the substitution in these analogues, the activities decreased in the order of **18** > **9** > **7** > **15** > **11** > **6** > **16** > **8** > **17** > **4** > **10** > **13** > **14** > **19**, indicating that grafting a pyrimidine ring at the 2, 3-positions with a hydrophobic group (=NH-8, $-NH_2$-9) is more beneficial to the activity than the other hydrophobic moieties at the 2-position of the 4*H*-benzo[*h*]chromene analogues.

Furthermore, the assessment of the impact of the substitution at the previous positions of the chromene systems against the HepG-2 cell line suggested that the order of the antiproliferative activities is diverse in accordance to the substitution type. For the 4*H*-benzo[*h*]chromene derivatives **4, 6–11, 13** and **14**, the activities were decreased in the order of **9** > **7** > **4** > **11** > **8** > **6** > **10** > **13** > **14**, while for the pyrimidine derivatives, the activities of compounds **15–19** were decreased in the order of **18** > **15** > **17** > **16** > **19**, intimating that the grafting of a lipophilic hydrophobic group, such as −N=CHOEt, at the 2-position with −CN-3 is more favourable than the fused pyrimidine ring at the 2, 3-positions of the 4*H*-benzo[*h*]chromene moiety.

3. Conclusion

β-enaminonitrile/ester (**7, 8, 10, 11, 13, 14**) and pyrimidines (**15–19**) derivatives have been synthesized, starting from *β*-enaminonitrile/ester (**4, 6**). The biological study was executed to analyse the outcome of the substituents and the pyrimidine rings on the antitumor behaviour. Most of the target compounds exhibited good antitumor activities towards the examined various tumour cell lines. Additionally, the presence of pyrimidine rings with hydrophobic groups such as = NH-8 or -Me-9 at the 2, 3-positions or the presence of hydrophobic groups such as −NHCOMe, −N=CHOEt, and $-N=CHNH_2$ at the 2-position with −CN-3 in the 4*H*-benzo[*h*]chromene system had a strong influence in the increase of the inhibitory activity of these molecules compared to that of the other hydrophobic and hydrophilic groups. In conclusion, the most active chromene derivatives, compounds **9**, **15**, and **18**, exhibited potent cytotoxic and antiproliferative effects on the three cancer cells through the caspase-dependent apoptosis mechanism. Moreover, these molecules caused a cancer cell capture in the S and G2/M − phases, and they were also able to inhibit cancer cell invasion and migration.

4. Experimental section

4.1. Chemistry

4.1.1. General

Solvents and reagents, as commercial-grade, were obtained from Sigma-Aldrich. Melting points were measured with a Stuart Scientific apparatus and are uncorrected. IR spectra were measured using a Jasco FT/IR 460 plus spectrophotometer. ^{1}H NMR and ^{13}C NMR spectra were recorded using a Bruker AV 500 MHz spectrometer. The ^{13}C NMR spectra were obtained using distortionless enhancement by polarization transfer (DEPT), where the signals of CH and CH_3 carbon atoms appear normal (up) and the signals of carbon atoms in CH_2 environments appear negative (down). The ^{13}C NMR spectra were also obtained using the attached proton test (APT); with this technique, the signals of CH and CH_3 carbon atoms appear normal (up) and the signals of CH_2 and Cq environments appear negative (down). Chemical shifts (δ) are expressed in parts per million (ppm)., while the MS spectra were measured using a Shimadzu GC/MS-QP5050A spectrometer. Elemental analyses were carried out at the Regional Centre for Mycology & Biotechnology, Al-Azhar University, Cairo, Egypt and the results were within ± 0.25%. Microwave synthesis was performed using a monomode Milestone Sr1 device. All the reactions are monitored using thin layer chromatography (TLC) on silica gel precoated F_{254} plates.

4.2. General procedure of chromene derivatives **4** and **6:**

4.2.1. 2-Amino-4-(3,4-dimethoxyphenyl)-6-methoxy-4H-benzo[h] chromene-3-carbonitrile **(4)** and Ethyl 2-amino-4-(3,4-dimethoxyphenyl)-6-methoxy-4H-benzo[h]chromene-3-carboxylate **(6)**

Starting materials were prepared according to previous reported procedure [50].

4.2.2. 2-Acetylamino-4-(3,4-dimethoxyphenyl)-6-methoxy-4H-benzo[h] chromene-3-carbonitrile **(7)**

Compound **4** (3.88 g, 0.01 mol) was refluxed in Ac_2O (20 mL) for ½ h or 6 h. The resulting product was collected and washed with cooled MeOH, and recrystallized from ethanol to afford **7** as a colourless solid; yield: 77%; mp 230–231 °C; $C_{25}H_{22}N_2O_5$ (430.45); calcd; %C: 69.76, %H: 5.15, %N: 6.51; found; %C: 69.81, %H: 5.18, %N: 6.56.

4.2.3. 2-Benzylideneamino-4-(3,4-dimethoxyphenyl)-6-methoxy-4H-benzo[h]chromene-3-carbonitrile **(8)**

Compound **4** (3.88 g, 0.01 mol), PhCHO (1.06 g, 0.01 mol), and piperidine (0.5 mL) was refluxed in ethanol (20 mL) for 2 h. (TLC monitoring). The formed product was recrystallized from ethanol/benzene to give **8** as a yellow solid; yield: 69%; mp 223–224 °C; $C_{30}H_{24}N_2O_4$ (476.52); calcd; %C: 75.61, %H: 5.08,%N: 5.88; found; %C: 75.57, %H: 5.02, %N: 5.81.

4.2.4. 2-Ethoxymethyleneamino-4-(3,4-dimethoxyphenyl)-6-methoxy-4H-benzo[h]chromene-3-carbonitrile **(9)**

The *β*-enaminonitrile **4** (3.88 g, 0.01 mol) with triethyl orthoformate (1.48 g, 0.01 mol) and Ac_2O (30 mL) was refluxed for 2 h., the resulting solid was recrystallized from benzene to give **9** as a yellow solid; yield: 85%; mp 146–147 °C; $C_{26}H_{24}N_2O_5$ (444.48); calcd; %C: 70.26, %H: 5.44, %N: 6.30; found; %C: 70.30, %H: 5.48, %N: 6.33.

4.2.5. 2-Dimethylaminomethyleneamino-4-(3,4-dimethoxyphenyl)-6-methoxy-4H-benzo[h]chromene-3-carbonitrile **(10)**

Method (a): The *β*-enaminonitrile **4** (3.88 g, 0.01 mol) with *N,N*-dimethylformamide dineopentyl acetal (2.31 g, 0.01 mol) and benzene (30 mL) was refluxed for 3 h., the resulting solid was recrystallized from benzene to give **10** as a colourless solid; yield: 89%; mp 184–185 °C; $C_{26}H_{25}N_3O_4$ (443.49); calcd; %C: 70.41, %H: 5.68, %N: 9.47; found; %C: 70.47, %H: 5.73, %N: 9.64.

Method (b): A mixture of imidate **9** (4.44 g, 0.01 mol) and Me_2NH (0.45 g. 0.01 mol) in methanol (30 mL) was stirred at room temperature for 1 h, then left overnight to precipitate. The solid product was recrystallized from benzene to afford **10** (m.p., mixed m.p., identical IR and MS spectrum).

4.2.6 2-Aminomethyleneamino-4-(3,4-dimethoxyphenyl)-6-methoxy-4H-benzo[h]chromene-3-carbonitrile (11)

Compound **11** was prepared from the imidate 9 (4.44 g, 0.01 mol) and NH_3 gas according to the procedure described for **10** (Method a). Compound **11** was recrystallized from ethanol to give **11** as a colourless solid; yield: 87%; m.p. 218–219 °C; $C_{24}H_{21}N_3O_4$ (415.44); calcd; %C: 69.39, %H: 5.10, %N: 10.11; found; %C: 69.44, %H: 5.14, %N: 10.15.

4.2.7 Ethyl 4-(3,4-dimethoxphenyl)-2-formamido-6-methoxy-4H-benzo[h]chromene-3-carboxylate (13)

Compound **13** was synthesized from **6** (4.35 g, 0.01 mol), triethyl orthoformate (1.48 g, 0.01 mol), and Ac_2O (30 mL) according to the procedure described for compound **9**. Compound **13** was recrystallized from benzene as a pale yellow solid; yield: 60%; mp 144–145 °C; $C_{26}H_{25}NO_7$ (463.48); calcd; %C: 67.38, %H: 5.44, %N: 3.02; found; %C: 67.41, %H: 5.50, %N: 3.05.

4.2.8 Ethyl 2-dimethylaminomethyleneamino-4-(3,4-dimethoxyphenyl)-6-methoxy-4H-benzo[h]-chromene-3-carboxylate (14)

Compound **14** was prepared from **6** (4.35 g, 0.01 mol), *N,N*-dimethylformamide dineopentyl acetal (2.31 g, 0.01 mol) and benzene (30 mL), according to the procedure described for compound **10**

(Method a). Compound **14** was recrystallized from benzene as a yellow solid; yield: 67%; mp 165–166 °C; $C_{28}H_{30}N_2O_6$ (490.55); calcd; %C: 68.56, %H: 6.16, %N: 5.71; found; %C: 68.60, %H: 6.21, %N: 5.75.

4.2.9 7-(3,4-Dimethoxyphenyl)-5-methoxy-7H,9H-benzo[h]chromeno[2,3–d]pyrimidin-8-one (15)

The *β*-enaminonitrile **4** (3.88 g, 0.01 mol) and HCO_2H (4.6 g, 1 mol) was refluxed for 3–5 h. (TLC monitoring) and the resulting solid was recrystallized from ethanol/benzene to give **15** as a colourless solid; yield: 88%; mp 180–181 °C; $C_{24}H_2ON_2O_5$ (416.43); calcd; %C: 69.22, %H: 4.84, %N: 4.84; found; %C: 69.19, %H: 4.75, %N: 6.64.

4.2.10 8-Amino-7-(3,4-dimethoxyphenyl)-5-methoxy-7H-benzo[h]chromeno[2,3–d]pyrimidine (16)

Compound **16** (4.15 g, 0.01 mol) was refluxed in EtOH in the presence of catalytic piperidine (0.5 mL) for 2 h. The formed precipitate was recrystallized from EtOH to give **16** as a colourless solid; yield: 79%; mp 207–208 °C; $C_{24}H_{21}N_3O_4$ (415.44); calcd; %C: 69.39, %H: 5.10, %N: 10.11; found; %C: 69.44, %H: 5.16, %N: 10.17.

4.2.11 7-(3,4-Dimethoxyphenyl)-5-methoxy-8-imino-9-methyl-7H-benzo[h]chromeno[2,3–d]pyrimidine (17)

Compound **17** was prepared from the imidate **9** (4.44 g, 0.01 mol), $MeNH_2$ (0.31 g, 0.01 mol), and MeOH (30 mL) according to the procedure described for compound **11**. Compound **17** was recrystallized from ethanol/benzene as a colourless solid; yield: 79%; mp 247–248 °C; $C_{25}H_{23}N_3O_4$ (429.47); calcd; %C: 69.92, %H: 5.40, %N: 9.78; found; %C: 70.00, %H: 5.48, %N: 9.81.

4.2.12 9-Amino-7-(3,4-dimethoxyphenyl)-5-methoxy-8-imino-7H-benzo[h]chromeno[2,3–d]pyrimidine (18)

Compound **18** was prepared from the imidate **9** (4.44 g, 0.01 mol), $NH_2NH_2{\cdot}2H_2O$ (0.5 g, 0.01 mol), and MeOH (30 mL) according to the procedure described for compound **11**. Compound **18** was recrystallized from benzene as a colourless solid; yield: 89%; mp 193–194 °C; $C_{24}H_{22}N_4O_4$ (430.46); calcd; %C: 66.97, %H: 5.15, %N: 13.02; found; %C: 66.90, %H: 5.07, %N: 12.95.

4.2.13 9-Benzylideneamino-7-(3,4-dimethoxyphenyl)-5-methoxy-8-imino-7H-benzo[h]-chromeno[2,3–d]pyrimidine (19)

The aminoimino compound **19** (4.30 g, 0.01 mol) and PhCHO (1.06 g, 0.01 mol) in EtOH (30 mL) and piperidine (0.5 mL) was refluxed for 2 h., the resulting solid was recrystallized from ethanol/benzene to give the open chain product **19** as a colourless solid; yield: 95%; mp 227–228 °C; $C_{31}H_{26}N_4O_4$ (518.56); calcd; %C: 71.80, %H: 5.05, %N: 10.80; found; %C: 71.85, %H: 5.13, %N: 10.92.

4.3. Biological screening

4.3.1. Cell lines

[Mammary gland breast cancer cell line (MCF-7), human Hepatocellular carcinoma (HepG-2) and human colon carcinoma (HCT-116)], chemicals used, crystal violent stain, Cell line Propagationand Cytotoxicity evaluation using viability assay are discussed in brief details in Supplementary materials section.

4.3.2. Cytotoxicity evaluation using viability assay

The cytotoxic activity was appraised using the 3-(4,5-dimethylthiazol-2-yl)-2,5-diphenyl tetrazolium bromide (MTT) colorimetric assay as reported previously [39,40].

4.3.3. Cell cycle analysis

Cell cycle arrest and distribution was assessed, using the Propidium Iodide Flow Cytometry Kit (ab139418, Abcam) followed by flow cytometry analysis. Briefly, 5×10^4 cells were seeded in 60 mm dishes and incubated for 24 h to form a cell monolayer. Cells were cultured for an additional 24 h in the absence (control) or presence of tested newly synthesized compounds **9**, **15**, and **18** (4 μg/mL). The adherent cells were trypsinized, washed with PBS, and fixed in 100% ice cold ethanol at +4 °C for at least 2 h. After again washing with PBS, cells were incubated with 200 μL 1X Propidium Iodide (PI) + RNase Staining Solution for 30 min at room temperature in the dark. The DNA content in each cell nucleus was determined by a FACS Calibur flow cytometer (BD Biosciences, Franklin Lakes, NJ, USA). Finally, cell cycle phase distribution was analysed using Cell Quest Pro software (BD Biosciences) showing collected propidium iodide fluorescence intensity on FL2.

4.3.4. Annexin V-FITC apoptosis assay

Apoptosis assay was performed with an Annexin V-FITC/PI double staining apoptosis detection kit (K101, BioVision) using a flow cytometer. The cell culture was prepared as reported for the cell cycle analysis assay with or without tested compounds (4 μg/mL). The staining procedure was performed following the manufacturer's instructions. A minimum of 10,000 cells per sample were acquired. Annexin V-FITC binding (FL1) and PI (FL2) were analysed using Cell Quest Pro software (BD Biosciences).

4.3.5. Caspase 3/7 activity assay

Caspase activity was measured after cell incubation for 24 h with compounds **9**, **15** and **18** (4 μg/mL) using the CellEvent™ Caspase 3/7 Green Flow Cytometry Assay Kit (C10427, Invitrogen). According to the manufacturer's instructions, 1 μL of CellEvent™ Caspase 3/7 Green Detection Reagent was added to flow cytometry tubes containing 1 mL of 5×10^4 treated cell/mL suspension and incubated for 30 min at 37 °C. Before the final 5 min of incubation, 1 μL of the 1 mM SYTOX™ AADvanced™ dead cell stain solution in DMSO was added. Stained samples were analysed by FACS Calibur flow cytometer (BD Biosciences, Franklin Lakes, NJ, USA).

4.3.6. DNA fragmentation

DNA fragmentation was quantitatively determined using diphenylamine (DPA) reagent according to the method of Boraschi and Maurizi [51]. Cells treated with tested compounds (4 μg/mL) for 24 h were harvested and centrifuged at 200*g* at 4 °C for 10 min., and the supernatant were transferred into a new tube labelled S while the pellet was moved into tube B. To allow the release of fragmented chromatin from nuclei, the cell pellet was resuspended in TTE lysis solution (Triton X-100 0.2%, Tris HCl 10 mM, EDTA 1 mM), vortexed, and centrifuged at 20,000*g* for 10 min at 4 °C. The new supernatants were transferred carefully to tubes labelled T. One mL of 25% TCA was added to tubes T, B, and S and allowed to precipitate by incubation overnight at 4 °C. The recovered precipitated DNA pellet was hydrolysed by adding 5% TCA to each pellet and heated for 15 min at 90 °C. A blank with 5% TCA alone was prepared. Solution of 320 μL of freshly prepared DPA was added to the sample, followed by incubation overnight at room temperature. The optical density was determined at 600 nm, and the percentage of DNA fragmentation was calculated as follows:

$$\%\text{Fragmented DNA} = \frac{\text{S+ T}}{\text{S+T+B}}\text{x100}$$

4.3.7. Cell invasion assay

Deregulated cell migration with compounds **9, 15** and **18** was performed using trans well chambers with non-coated membranes (96-well HTS Trans well Permeable Supports with 8 μm pores, Cat. No. 3374, Corning, Life Sciences). For invasion assays, 5×10^4 cells from treated cell lines were plated in the top chamber with Matrigel-coated membrane. Medium without serum was added to the upper chamber, and the medium containing 10% foetal bovine serum was added into the lower chamber. After 48 h, the cells were fixed in 10% neutral buffered formalin solution for 30 min and stained with 0.05% crystal violet solution for 30 min, and the cells that invaded through the pores to the lower surface of the inserts were counted under a phase contrast inverted microscope.

4.3.8. Statistics

All data were expressed as the means ± standard deviation (SD) from at least three independent experiments with similar results. Statistical analysis was performed by GraphPad Prism 5.01 (GraphPad software, San Diego, CA, USA). Experiments were analysed using ANOVA followed by Tukey's post hoc test. Statistical significance is indicated as $^{*}\mathbf{p} \leq \mathbf{0.05}$, $^{**}\mathbf{p} \leq \mathbf{0.01}$, **and** $^{***}\mathbf{p} \leq \mathbf{0.001}$.

Acknowledgements

The authors profoundly thank Al-Azhar University for carrying out the antitumor study and elemental analyses.

Appendix A. Supplementary material

Supplementary data to this article can be found online at https://doi.org/10.1016/j.bioorg.2019.03.059.

References

[1] H.K. Abd El-Mawgoud, H.A.M. Radwan, F. El-Mariah, A.M. El-Agrody, Characterization Synthesis, Biological activity of novel 1*H*-benzo[*f*]chromene and 12*H*-benzo[*f*]chromeno[2,3-*d*]pyrimidine derivatives, Lett. Drug. Des. Discov. 15 (2017) 857–865.
[2] T.H. Afifi, R.M. Okasha, H.E.A. Ahmed, J. Ilas, T. Saleh, A.S. Abd-El-Aziz, Structure-activity relationships and molecular docking studies of chromene and chromene based azochromophores: a novel series of potent antimicrobial and anticancer agents, Excli j. 16 (2017) 868–902.
[3] G. Singh, A. Sharma, H. Kaur, M. Ishar, Chromanyl-isoxazolidines as antibacterial agents: synthesis, biological evaluation, quantitative structure activity relationship, and molecular docking studies, Chem. Biol. Drug. Des. 87 (2016) 213–223.
[4] C. Bingi, N.R. Emmadi, M. Chennapuram, Y. Poornachandra, C.G. Kumar, J.B. Nanubolu, K. Atmakur, One-pot catalyst free synthesis of novel kojic acid tagged 2-aryl/alkyl substituted-4*H*-chromenes and evaluation of their antimicrobial and anti-biofilm, Bioorg. Med. Chem. Lett. 25 (2015) 1915–1919.
[5] J. Yeh, M. Coumar, J. Horng, H. Shiao, F. Kuo, H. Lee, I. Chen, C. Chang, W. Tang, S. Tseng, C. Chen, S. Shih, J. Hsu, C. Liao, Y. Chao, H. Hsieh, Anti-influenza drug discovery: structure-activity relationship and mechanistic insight into novel angelicin derivatives, J. Med. Chem. 53 (2010) 1519–1533.
[6] J. Chen, J. Cho, T. Hwang, I. Chen, Benzoic acid derivatives, acetophenones, and anti-inflammatory constituents from melicopesemecarpifolia, J. Nat. Prod. 71 (2008) 71–75.
[7] S. Cheng, K. Huang, S. Wang, Z. Wen, P. Chen, C. Duh, Antiviral and anti-inflammatory metabolites from the soft coral *Sinularia capillosa*, J. Nat. Prod. 73 (2010) 771–775.
[8] W. Gregor, G. Grabner, C. Adelwohrer, T. Rosenau, L. Gille, Antioxidant properties of natural and synthetic chromanol derivatives: study by fast kinetics and electron spin resonance spectroscopy, J. Org. Chem. 70 (2005) 3472–3482.
[9] C. Bruhlmann, F. Ooms, P. Carrupt, B. Testa, M. Catto, F. Leonetti, C. Altomare, A. Cartti, Coumarins derivatives as dual inhibitors of acetyl cholinesterase and monoamine oxidase, J. Med. Chem. 44 (2001) 3195–11398.
[10] Y.M. Cui, M.Z. Ao, W. Li, L.J. Yu, Effect of glabridin from Glycyrrhizaglabra on learning and memory in mice, Planta Med. 74 (2008) 377–380.
[11] J. Kim, C. Kim, Y. Lee, E. Sohn, K. Jo, S. Shin, J.S. Kim, Scopoletin inhibits rat aldose reductase activity and cataractogenesis in galactose-fed rats, Evid. Based Complement. Altern. Med. (2013) 1–8. Article ID 787138.
[12] M. Costa, T.A. Dias, A. Brito, F. Proença, Biological importance of structurally diversified chromenes, Eur. J. Med. Chem. 123 (2016) 487–507.
[13] V.Y. Korotaev, V.Y. Sosnovskikh, A.Y. Barkov, Synthesis and properties of 3-nitro-2*H*- Chromenes, Russ. Chem. Rev. 82 (2013) 1081–1116.
[14] S.A. Patil, R. Patil, L.M. Pfeffer, D.D. Miller, Chromenes: potential new chemotherapeutic agents for cancer, Future Med. Chem. 5 (2013) 1647–1660.
[15] D. Tiana, S. Dasa, J. Doshia, J. Pengb, J. Linb, C. Xing, sHA 14–1, a stable and ROS-free antagonist against anti-apoptotic Bcl-2 proteins, bypasses drug resistances and synergizes cancer therapies in human leukemia cell, Cancer Lett. 259 (2008) 198–208.
[16] D. Hermanson, S. Addo, A. Bajer, J. Marchant, S. Das, B. Srinivasan, F. AlMousa, F. Michelangeli, D. Thomas, T. LeBien, C. Xing, Dual mechanisms of sHA 14–1 in inducing cell death through endoplasmic reticulum and mitochondria, Mol. Pharmacol. 76 (2009) 667–678.
[17] S. Das, J. Doshi, D. Tian, S. Addo, B. Srinivasan, D. Hermanson, C. Xing, Structure-activity relationship and molecular mechanisms of ethyl 2-amino-4-(2-ethoxy-2-oxoethyl)-6-phenyl-4*H*-chromene-3-carboxylate (sHA 14–1) and its analogues, J. Med. Chem. 52 (2009) 5937–5949.
[18] S. Das, B. Srinivasan, D. Hermanson, N. Bleeker, J. Doshi, R. Tang, W. Beck, C. Xing, Structure-activity relationship and molecular mechanisms of ethyl 2-amino-6-(3,5-dimethoxyphenyl)-4-(2-ethoxy-2-oxoethyl)-4*H*-chromene-3-carboxylate (CXL017) and its analogues, J. Med. Chem. 54 (2011) 5937–5948.
[19] W. Kemnitzer, J. Drewe, S. Jiang, Discovery of 4-aryl-4*H*-chromenes as a new series of apoptosis inducers using cell- and caspase based high-throughput screening assay. 1. Structure-activity relationships of the 4-aryl group, J. Med. Chem. 47 (2004) 6299–6310.
[20] S.A. Patil, J. Wang, X.S. Li, New substituted 4*H*-chromenes as anticancer agents, Bioorg. Med. Chem. Lett. 22 (2012) 4458–4461.
[21] M. Mahmoodi, A. Aliabadi, S. Emami, Synthesis and *in vitro* cytotoxicity of polyfunctionalized 4-(2-arylthiazol-4-yl)-4*H*-chromenes, Arch. Pharm. Chem. Life Sci. 343 (2010) 411–416.
[22] T. Akbarzadeh, A. Rafinejad, J.M. Mollaghasem, 2-amino-3-cyano-4-(5-arylisoxazol-3-yl)- 4*H*-chromenes: synthesis and in vitro cytotoxic activity, Arch. Pharm. Chem. LifeSci. 345 (345) (2012) 386–392.
[23] A.M. Shestopalov, Y.M. Litvinov, L.A. Rodinovskaya, O.R. Malyshev, M.N. Semenova, V.V. Semenov, Polyalkoxy substituted 4*H*-chromenes: synthesis by domino reaction and anticancer activity, ACS Comb. Sci. 14 (2012) 484–490.
[24] A.M. El-Agrody, A.H. Halawa, A.M. Fouda, A.M. Al-Dies, Antiproliferative activity of novel 4*H*-benzo[*h*]chromenes, 7*H*-benzo[*h*]chromeno[2,3-*d*]pyrimidines and the structure-activity relationships of the 2-, 3-positions and fused rings at the 2, 3-positions, J. Saudi. Chem. Soc. 21 (2017) 82–90.
[25] A.H. Halawa, A.M. Fouda, A.M. Al-Dies, A.M. El-Agrody, Synthesis, biological evaluation and molecular docking studies of 4*H*-benzo[*h*]chromenes, 7*H*-benzo[*h*]chromeno[2,3-*d*]pyrimidines as antitumor agents, Lett. Drug. Des. Discov. 13 (2016) 77–88.
[26] A.M. El-Agrody, A.M. Fouda, A.M. Al-Dies, Studies on the synthesis, *in vitro* antitumor activity of 4*H*-benzo[*h*]chromene, 7*H*-benzo[*h*]chromeno[2,3-*d*]pyrimidine derivatives and structure activity relationships of the 2-,3- and 2,3-positions, Med. Chem. Res. 23 (2014) 3187–3199.
[27] R.M. Okasha, F.F. Alblewi, T.H. Afifi, A. Naqvi, A.M. Fouda, A.M. Al-Dies, A.M. El-Agrody, Design of new benzo[*h*]chromene derivatives: antitumor activities and structure-activity relationships of the 2,3-positions and fused rings at the 2,3-positions, Molecules 22 (2017) 479–496.
[28] A. Kheirollahi, M. Pordeli, M. Safavi, S. Mashkouri, M.R. Naimi-Jamal, S.K. Ardestani, Cytotoxic and apoptotic effects of synthetic benzochromene derivatives on human cancer cell lines, Naunyn-Schmiedeberg's Arch Pharmacol 387 (2014) 1199–1280.
[29] A. Rafinejad, A. Fallah-Tafti, R. Tiwari, A.N. Shirazi, D. Mandal, A. Shafiee, K. Parang, Ali Foroumadi, T. Akbarzadeh, 4-Aryl-4*H*-naphthopyrans derivatives: one-pot synthesis, evaluation of Src kinase inhibitory and anti-proliferative activities, DARU J. Pharm. Sci. 20 (2012) 100–107.
[30] S. Gorle, S. Maddila, S.N. Maddila, K. Naicker, M. Singh, P. Singh, S.B. Jonnalagadda, Synthesis, molecular docking study and in vitro anticancer activity of tetrazole linked benzochromene derivatives, Anti-Cancer Agents in Med. Chem. 17 (2017) 464–470.
[31] H.E.A. Ahmed, M.A.A. El-Nassag, A.H. Hassan, R.M. Okasha, S. Ihmaid, A.M. Fouda, T.H. Afifi, A. Aljuhani, A.M. El-Agrody, Introducing novel potent anticancer agents of 1*H*-benzo[*f*]chromene scaffolds, targeting *c-Src* kinase enzyme with MDA-MB-231 cell line anti-invasion effect, J. Enzyme Inhibition Med. Chem. 33 (2018) 1074–1088.
[32] S. Nowsheen, E.S. Yang, The intersection between DNA damage response and cell death pathways, Exp. Oncol. 34 (2012) 243–254.
[33] A.M. El-Agrody, H.K. Abd El-Mawgoud, A.M. Fouda, E.S.A.E.H. Khattab, Synthesis in-vitro cytotoxicity of 4*H*-benzo[*h*]chromene derivatives and structure-activity relationships of 4-aryl group and 3-, 7-positions, Chem. Pap. 70 (2016) 1279–1292.
[34] M.M. Khafagy, A.H.F. Abd El-Wahab, F.A. Eid, A.M. El-Agrody, Synthesis of halogen derivatives of benzo[*h*]cheromene and Benzo[*a*]anthracene with promising antimicrobial activities, IL Farmaco 57 (2002) 715–722.
[35] D. Panda, J.P. Singh, L. Wilson, Suppression of microtubule dynamics by LY290181 a potential mechanism for its antiproliferative action, J. Biol. Chem. 272 (1997) 7681–7687.
[36] D.L. Wood, D. Panda, T.R. Wiernicki, L. Wilson, M.A. Jordan, J.P. Singh, Inhibition of mitosis and microtubule function through direct tubulin binding by a novel antiproliferative naphthopyran LY290181, Mol. Pharmacol. 52 (1997) 437–444.
[37] A.M. El-Agrody, A.M. Fouda, E.S.A.E.H. Khattab, Synthesis antitumor activity of 2-amino-4*H*-benzo[*h*]chromene derivatives and structure-activity relationships of the 3- and 4-positions, Med. Chem. Res. 22 (2013) 6105–6120.
[38] A.M. El-Agrody, A.M. Fouda, E.S.A.E.H. Khattab, Halogenated 2-amino-4*H*-benzo[*h*]-chromene derivatives as antitumor agents and the relationship between lipophilicity and antitumor activity, Med. Chem. Res. 26 (2017) 691–700.
[39] T. Mossman, Rapid colorimetric assay for cellular growth and survival: application to proliferation and cytotoxicity assays, J. Immunol. Methods 65 (1983) 55–63.
[40] A.U. Rahman, M.I. Choudhary, W.J. Thomsen, Bioassay Technique for Drug Development, ISBN 0-203-34349-2 Harwood Academic Publishers, 2001.
[41] C.P. Harish, K.K. Santosh, Cryptolepine, a plant alkaloid, inhibits the growth of non-melanoma skin cancer cells through inhibition of topoisomerase and induction of DNA damage, Molecules 21 (2016) 1758–1775.
[42] B.L. Staker, M.D. Feese, M. Cushman, Y. Pommier, D. Zembower, L. Stewart, A.B. Burgin, Structures of three classes of anticancer agents bound to the human topoisomerase I-DNA covalent complex, J. Med. Chem. 7 (2005) 2336–2345.
[43] V.A. Fadok, D.R. Voelker, P.A. Campbell, J.J. Cohen, D.L. Bratton, P.M. Henson, Exposure of phosphatidylserine on the surface of apoptotic lymphocytes triggers specific recognition and removal by macrophages, J. Immunol. 1 (1992) 2207–2216.
[44] S. Elmore, Apoptosis: a review of programmed cell death, Toxicol. Pathol. 35 (2007) 495–516.
[45] F.H. Igney, P.H. Krammer, Death and anti-death: tumor resistance to apoptosis, Nat. Rev. Cancer. 2 (2002) 277–288.
[46] C.M. Henry, E. Hollville, S.J. Martin, Measuring apoptosis by microscopy and flow cytometry, Methods 61 (2013) 90–97.

[47] A. Beberok, D. Wrześniok, J. Rok, Z. Rzepka, M. Respondek, E. Buszman, Ciprofloxacin triggers the apoptosis of human triple-negative breast cancer MDA-MB-231 cells via the p53/Bax/Bcl-2 signaling pathway, Int. J. Oncol. 52 (2018) 1727–1737.
[48] I. Kaverina, A. Straube, Regulation of cell migration by dynamic microtubules, Semin Cell Dev. Biol. 22 (2011) 968–974.
[49] C. Rooney, G. White, A. Nazgiewicz, S.A. Woodcock, K.I. Anderson, C. Ballestrem, The Rac activator STEF (Tiam2) regulates cell migration by microtubule-mediated focal adhesion disassembly, EMBO Rep. 11 (2010) 292–298.
[50] A.M. El-Agrody, A.M. Fouda, A.M. Al-Dies, Microwave assisted synthesis of 2-amino-6-methoxy-4*H*-benzo[*h*]chromene derivatives, Europ. J. Chem. 5 (2014) 133–137.
[51] D. Boraschi, G. Maurizi, Quantitation of DNA fragmentation with diphenylamine, in: D. Boraschi, P. Bossù, A. Cossarizza (Eds.), Apoptosis – A Laboratory Manual of Experimental Methods, GCI Publications, L'Aquila, 1998, pp. 153–161.